

The effect of hydrothermal grown zinc oxide nanoparticles as seeds on the properties of nanoripples in zinc oxide thin films

M Seabi^{1,a,*}, T Muller^{1,b}, S Bolokang^{2,1,c}, F Cummings^{3,d}, C Arendse^{1,e}

¹ Department of Physics and Astronomy, University of the Western Cape, Robert Sobukwe Road, Bellville 7530, South Africa

² Advanced Casting Technologies, Light Metals, Materials Science & Manufacturing, Council for Scientific and Industrial Research, Meiring Naudé Road, Brummeria, Pretoria 0185, South Africa

³ Electron Microscope Unit, University of the Western Cape, Robert Sobukwe Road, Bellville 7530, South Africa

Email: ^a3868098@myuwc.ac.za*, ^btmuller@uwc.ac.za, ^csbolokang@csir.co.za, ^dfcummings@uwc.ac.za, ^ecarendse@uwc.ac.za

Abstract

This work reports on a simple approach to improving the optoelectronic properties of Wurtzite ZnO nanoripples by means of incorporating hydrothermally synthesised ZnO nanoparticles under controlled synthesis temperature. Initially, ZnO nanoparticles were investigated and subsequently utilised as seeds to induce ripple growth in spin-coated ZnO thin films. TEM images illustrated the development of nanospheres at 140°C. The yield of ZnO NPs at 180°C increased and consisted of a combination of nanorods and nanospheres. Morphologically, seedless ZnO nanoripples showed rugged ends of the nanoripple structures. The SEM images illustrated that the layers uniformly formed on the substrates, and seeding the ZnO nanoripples caused the nanoripples to elongate. The thickness of the nanoripples thin films showed a decrease with the incorporation of hydrothermally synthesised ZnO seeds from 134 nm for unseeded ZnO nanoripples to 96 nm at 180°C. The incorporation of ZnO NPs seeding treatment increased the transmission of ZnO nanoripples from 82% to 92%, leading to untreated ZnO nanoripples exhibiting a direct band gap of 3.19 eV that increased after seeding to 3.36 eV. The change in the band gap to a higher value(s) and increased transparency confirms the progressive improvement of the thin films due to incorporating ZnO seeding for optoelectronic and photovoltaic applications.

Keywords: Hydrothermal Method, Nanoparticles, Nanoripples, Thin Films, Zinc oxide

1. Introduction

Semiconductors whose dimensions are nanometre size play a significant role in electronic, photovoltaic, biological sensing, and optical device applications. This is due to their electrical, optical, and chemical properties, which can be tuned by changing the size of the particles.¹ Zinc oxide (ZnO) is an n-type semiconductor with a direct band gap; it comprises a considerable fraction of ionic bonding.^{2,3} ZnO has attracted the research field due to its typical and novel properties, such as a wide band gap of 3.37 eV and exciton energy of 60 meV.⁴ Owing to its ability to be effectively used in solid-state light sources and detectors in the blue and UV region of the electromagnetic spectrum, ZnO occupies a unique position among wide energy band gap semiconductors such as gallium nitride and zinc sulphide.² ZnO is applied in different fields of science and technology.⁴ Areas such as light-emitting diodes, UV detectors, high sensitive gas sensors,⁵ solar cells,⁶ laser diodes, and photoluminescent devices.^{4,7} Recently, various methods have produced ZnO powders and thin film structures of controlled morphology and sizes.⁴ Current techniques for synthesising ZnO nanostructures include chemical vapour deposition (CVD), electrophysical deposition, hydrothermal synthesis, electrochemical synthesis, solution combustion, sol-gel technique, and co-precipitation method.⁴ Hydrothermal synthesis is the promising alternative synthetic method for nano-sized semiconductors due to its low process temperature and its easy route to control particle size.⁷

Moreover, hydrothermal synthesis uses simple equipment, catalyst-absence growth, low-cost and environmental friendliness.⁷ The hydrothermal method is applied in microelectronics and plastic electronic manufacturing due to its low reaction temperatures. This synthetic technique has been employed to prepare ZnO nanoparticles and other semiconductors successfully. The nanoparticle's crystalline size, morphology, and optical properties can be tuned via the hydrothermal synthesis process by adjusting the precursors' reaction temperature, time, and concentration.¹ In the present study, the effect of hydrothermally synthesised ZnO NPs as seeds at various temperature conditions on the ZnO nanoripples' structural, morphological, and optical properties was investigated and presented.

2. Experimental

2.1 Synthesis of ZnO NPs, unseeded ZnO NRs, and seeded ZnO NRs

All reagents were analytically pure and used without further purification. To synthesise ZnO NPs, a stock solution of 2M zinc acetate dihydrate (99.99% purity) was prepared in 50 ml methanol while stirring. To the stirring stock solution, 0.5M sodium hydroxide solution prepared in 15 ml methanol was added. The solution was left to go for 30 min. As the solution reached a pH of ~11, it was removed and transferred to a Teflon-lined sealed stainless steel autoclave at 140°C and 180°C. Post reaction completion, the resultant white solids were removed. The solids were washed with ethanol, deionised water, and then centrifuged at

12 000 rpm for 10 min. The washing steps were repeated ten times to remove impurities. The washed products were left to dry at 60°C overnight in the oven and packaged in vials.

To produce ZnO-based nanoripples, 0.75M zinc acetate dihydrate was dissolved in 63 ml of 2-methoxyethanol, and 2.62 ml of ethanolamine was added to stabilise the Zn (II) ions by facilitating Zn (II) chelation. The solution was left to stir at 60°C for 30 min. Afterward, the solution was divided, and from the two batches of ZnO NPs, 0.25 mg of ZnO NPs was drawn from each sample and dissolved in 21 ml of the zinc acetate solution. Two vials were prepared, containing a combination of ZnO NPs synthesised at 140°C and 180°C and zinc acetate solution. In preparation for the thin film deposition, the clear quartz substrates were immersed in IPA, acetone, isopropanol, ethanol, and DI water at 60°C and sonicated for 15 min each. Compressed nitrogen gas was used to dry the samples after sonication. The thin films were prepared by spin coating the 0.40 μ L of each solution at 2000 rpm for 40 s using an Ossila spin coater and ramp-annealed from room temperature to 275°C using a Chemat (Technology Inc) hotplate.

2.2 Characterisation

A Bruker D8-advanced-8-X-ray powder diffractometer with CuK_α radiation ($\lambda=1.54050 \text{ \AA}$) was used to study the crystallinity and crystal phase of ZnO NPs. The Bragg angle ranges from 25° to 85° with a typical step size of 0.034°. An FEI Tecnai G2 20 field-emission gun (FEG) High-resolution transmission electron microscope (HRTEM) was employed to study the crystallinity, size, and morphological properties of ZnO NPs.

A Zeiss Auriga emission gun SEM (FEG-SEM) was employed to study the morphological properties of the ZnO-based nanoripples thin films. The electrons' accelerating voltage was set to 5 kV during operation, and secondary electron images were collected with an in-lens detector. Transmittance spectroscopy was utilised to study the optical properties of the ZnO-based nanoripples thin films. Measurements were collected with a Semiconsoft UV-vis spectrometer over a spectral range of 200 nm to 900 nm.

3. Results and discussion

Fig 1 shows the X-ray diffraction patterns of the ZnO nanopowders produced at 140°C and 180°C, respectively. XRD technique helps to determine the crystal size, sample purity, lattice parameters, and strain due to lattice dislocation. The XRD peaks indicate the high purity of the synthesised ZnO NPs as no foreign phases are detected. These XRD patterns have been indexed as the hexagonal wurtzite phase of ZnO⁸ with reported lattice constants $a=b= 3.24 \text{ \AA}$ and $c= 5.21 \text{ \AA}$ (JPCDS card number: 00-036-1451)⁸. XRD plots of intensity versus 2θ show sharp peaks (Fig 1) corresponding to particles having crystalline sizes of 21.5 and 21.6 nm corresponding to ZnO NPs synthesised at 140°C and 180°C, respectively.⁹ The intensity of the (101) plane is found to be relatively intense for all the samples. Therefore, the preferred orientation is along the [101] axis.¹⁰

The interplanar distance was calculated according to Bragg's law (3.1), and the crystallite sizes of the maximally intense (101) peaks were estimated using the Debye-Scherrer's formula (3.2).⁹ The

lattice strain due to crystal defect and deformation is evaluated using equation (3.3):¹¹

$$d_{hkl} = n\lambda\sin\theta, \quad (3.1)$$

$$D = \frac{k\lambda}{\beta_{hkl}\cos\theta}, \quad (3.2)$$

$$\varepsilon = \frac{\beta_{hkl}}{4\tan\theta}, \quad (3.3)$$

here D is the crystallite size, 0.89 is the Scherrer's constant k for spherical particles, λ is the wavelength of the type of incident radiation, θ is the Bragg diffraction angle, and β is the full width at half-maximum (FWHM) of the diffraction peak (101),⁷ and ε is the lattice strain. The lattice parameters were calculated from equation (3.3),

$$\frac{1}{d_{hkl}^2} = \frac{4}{3[a^2(h^2+hk+k^2)]} + \frac{l^2}{c^2} \quad (3.3)$$

where d_{hkl} is the interplanar spacing for the plane (101), a and c are the lattice parameters, and h , k , and l are the Miller indices (7).⁷ The (101) plane was used to make a quantitative analysis presented in Table 1. Table 1 shows the estimated crystallite sizes, lattice parameters, and lattice strain of ZnO NPs fabricated at 140°C and 180°C, respectively. Therefore, the lattice dislocations found in the sample are associated with the strain calculated and the change in the crystallite size. This is supported by the deviation in the lattice parameters values from the reported values,⁸ outlined in Table 1. However, the c/a ratios shown in Table 1 for the two ZnO NPs samples are 1.61. This axial ratio value confirms that the atoms of the two ZnO NPs samples are closely packed, just as in an ideal ZnO hexagonal close-packed crystal value at 1.60.⁷

HRTEM images of hydrothermally grown ZnO samples are shown in Fig 2 (a) and (b). The average particle sizes were calculated; the histograms alongside the SAED micrographs are presented in Fig 2 (a) and (b) inset. A combination of primarily spherical nanostructures and a small yield of nanorods is observed in Fig 2 (a). An increase in temperature to 180°C (Fig 2 (b)) resulted in a combination of primarily nanorods and secondarily sphere-

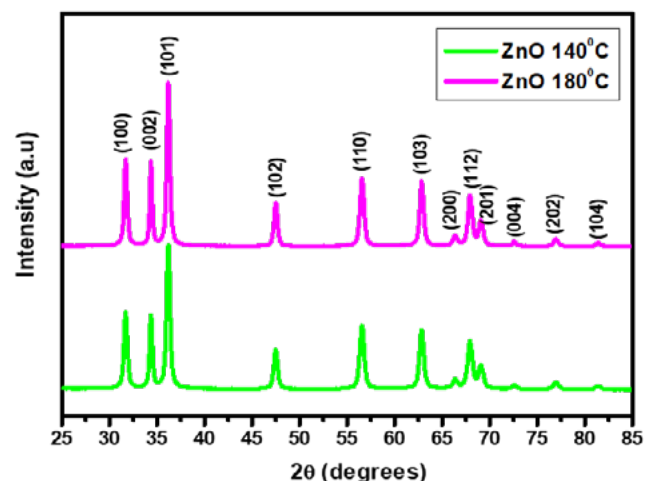


Figure 1: (a) XRD pattern of ZnO NPs synthesized 140°C and 180°C, respectively

Table 1: A summary of the estimated lattice parameters, calculated crystallite size, and microstrain for ZnO synthesised 140°C and 180°C, respectively

Sample	Lattice parameters (Å)			(Crystallite size)	Lattice Strain
	a	c	c/a	D (nm)	
ZnO NPs (140°C)	3.25	5.23	1.61	21.5	5.90×10^{-4}
ZnO NPs (180°C)	3.23	5.21	1.61	21.6	5.95×10^{-4}

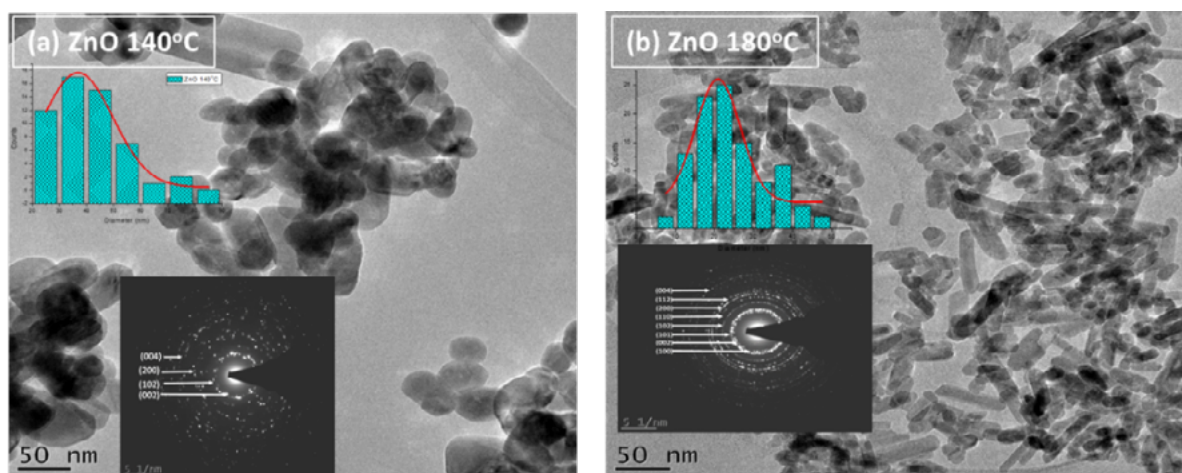


Figure 2: TEM images of ZnO NPs fabricated at 140°C and 180°C. The inset show diameter distributions and SAED images

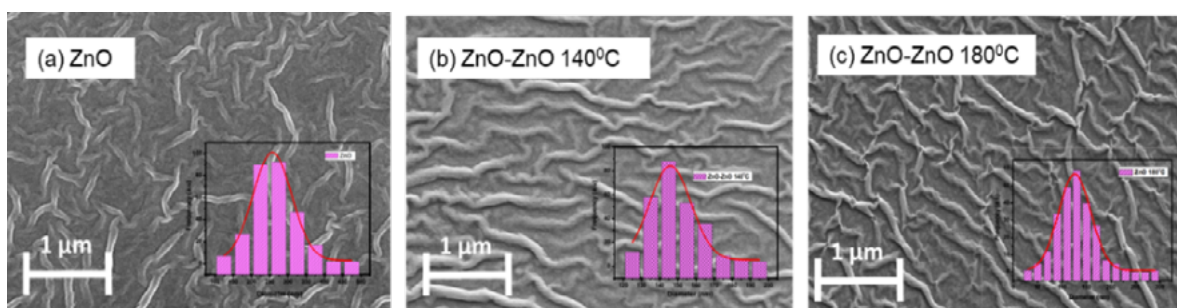


Figure 3: SEM images of (a) unseeded ZnO NRs, (b) and (c) seeded ZnO NPs-ZnO NRs, synthesised with bare zinc acetate solution combined with ZnO NPs synthesised at 140°C and 180°C, respectively. The inset images show the diameter distribution of the nanoripples

shaped ZnO NPs. The particle sizes of these samples decrease from 36.9 nm to 15.7 nm with increasing temperature. The inset of the histograms demonstrates this in Fig 2 (a) and (b), and it is consistent with the reported ZnO structure of Sonima Mohan et al.¹⁰ The observed diffraction spots and ring patterns in SAED micrographs were indexed with the assistance of bulk ZnO JCPDS card 00-036-1451 data.⁸ The SAED patterns illustrate that the samples are hexagonal wurtzite ZnO structures in crystallography, which agrees with XRD results. Their particle size determined from TEM analysis of ZnO NPs at 140°C is greater than the Scherrer method-extracted crystallite size in XRD analysis. Furthermore, the particle size of ZnO NPs at 180°C was found to be less than the crystallite size. The intensity of the diffraction rings increases with the synthesis temperature of the ZnO NPs, which suggests an increase in the polycrystallinity of the nanomaterials.⁷

The morphology and diameter distribution of the unseeded ZnO NRs and seeded ZnO NRs fabricated from a combination of hydrothermally synthesised ZnO nanoparticles at 140°C and 180°C, and bare zinc acetate solution NRs are presented in the

SEM images in Fig 3 (a)-(c). Seedless ZnO nanoripples show contracted nanoripple structures with rugged ends. SEM images illustrated that seeding the ZnO nanoripples causes the nanoripples to elongate and uniformly form on the substrate. Furthermore, an increase in the temperature of the seeding nanoparticles causes a decrease in the diameter distribution of the nanoripples (Fig 3 (a) and (b) inset). The diameter distribution of unseeded ZnO NRs is 320.4 ± 86.0 nm, ZnO-ZnO 140°C NRs is 246.4 ± 74.7 nm, and ZnO-ZnO 180°C NRs 125.8 ± 33.0 nm. Seeding the nanoripples causes the thin film to decrease in thickness. The thickness values of the thin films were found to be 188, 100, and 96 nm for unseeded ZnO NRs, ZnO-ZnO 140°C, and ZnO-ZnO NRs 180°C, respectively. The decrease in the thickness attributes to the transparency in thin films. An increase in transparency is beneficial for optoelectronic applications as absorption of charge carriers increases due to high transparency.¹²

The UV-Visible absorbance spectra, transmittance spectra, and Tauc plots of the unseeded ZnO nanoripple thin film structures and seeded ZnO-ZnO 140°C NRs, and ZnO-ZnO 180°C NRs

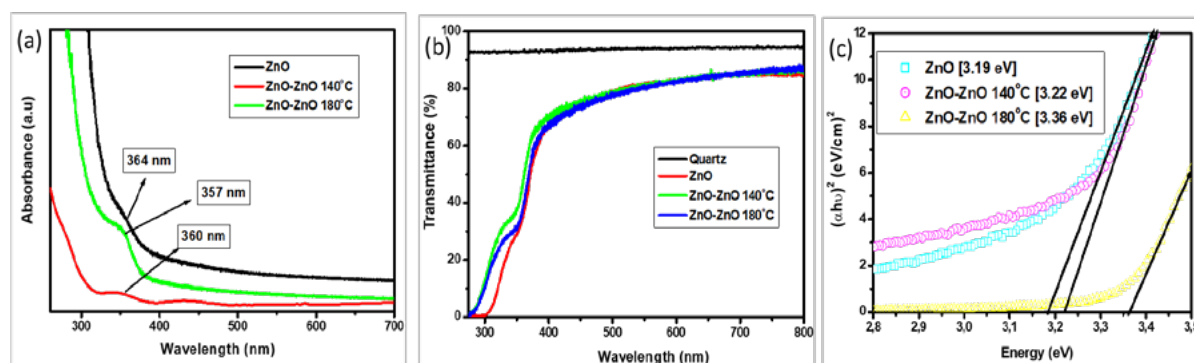


Figure 4: (a) the absorbance spectra (b), UV–Vis transmittance plots spectra, and (c) the Tauc plots representing direct band gap values the unseeded ZnO NRs and seeded ZnO NPs-ZnO NRs synthesised with bare zinc acetate solution combined with ZnO NPs synthesised at 140°C and 180°C, respectively

synthesised on quartz substrates are shown in Fig 4 (a), (b), and (c) respectively.

The absorption spectra (Fig 4 (a)) show near UV absorption at ~357, ~364, and ~360 nm for ZnO NRs, ZnO-ZnO 140°C NRs, and ZnO-ZnO 180°C NRs, respectively. This change is a blue-shift compared to the bulk value (~375 nm)¹⁰ and is attributed to the intrinsic defects. All the samples fabricated show transmission of $T > 75\%$ at the longer wavelength of $\lambda > 550$ nm in the visible region of the electromagnetic spectrum (Fig 4 (b)). The transparency is attributed to the morphology alteration of the NRs due to the incorporation of ZnO nanoparticles. Band gap values for the three samples were determined from Tauc plots. The values were extrapolated from the linear portion of the x-axis of $(\alpha h\nu)^{1/2}$ versus $h\nu$ plot as $(\alpha h\nu)^{1/2}$ approaches zero, shown in Fig 4 (c). The obtained values are 3.19, 3.22, and 3.36 eV for unseeded ZnO NRs, ZnO-ZnO 140°C NRs, and ZnO-ZnO 180°C NRs respectively. In optoelectronics, large band gap value(s) of ZnO nanostructured thin films ranging from 3.0-3.4 eV are essential for effective working devices.¹³ For example, Yong-Jin Noh et al.¹⁴ optimised ZnO nanostructures for inverted polymer solar cells application. The optimised ZnO layer exhibit a band gap of ~3.2 eV and an efficiency of 4.22%. Therefore, the optimised ZnO layer in inverted organic cells is recognised as a potential material for the electron transport layer to substitute TiO_2 . Thus, the band gap values found in this study ranging from 3.19 to 3.36 eV agree with the intrinsic band gap of 3.37 eV.¹⁰ The increasing band gap with increased NPs' synthesis temperature leads to a change in the Plasmon absorption region that is attributed to the ZnO NPs aggregation.⁷

4. Conclusion

ZnO NPs were fabricated by the hydrothermal method under various reaction temperature values to study the effect of the synthesised ZnO NPs as seeds on the properties of ZnO NRs. In the analysis, TEM images revealed that hydrothermal synthesis of ZnO NPs at different temperature values results in NPs of various shapes. The particle size values were found to be less than the crystallite sizes obtained in XRD. The unseeded ZnO NRs thin films showed a diameter distribution of 320.4 ± 86.0 nm, which decreased as the temperature of the ZnO NPs seeds increased. Adding the ZnO NPs produced at 140°C and 180°C leads to a decrease in the diameter distributed along the area. All the thin films were fabricated with 0.40 μL , yet each sample resulted in different thicknesses, illustrating that the thin films are highly affected by adding the ZnO NPs seeds. Therefore, a change in the

UV/Vis absorption occurred, and the seeded samples showed a blue shift compared to the unseeded sample, with band gap values ranging from ~3.19-3.36 eV. This analysis suggests that adding ZnO NPs in the fabrication of ZnO NRs improves the properties of ZnO NRs thin films. Therefore, ZnO NPs-ZnO NRs may be used as a potential material for optoelectronic applications.

Acknowledgments

This work was financially supported by the Nanoscience Postgraduate Programme, South Africa. The authors would like to acknowledge iThemba labs, Faure, Cape Town, the CSIR group, The University of the Western Cape Microscope Unit, and Siyabonga Mdluli at UWC Chemical Sciences measurement assistance.

References

1. Aneesh PM, Vanaja KA, Jayaraj MK. 2007. Synthesis of ZnO nanoparticles by hydrothermal method, *Optoelectronic Devices Laboratory*, Vol. 6639, pp. 1-9.
2. Rodnyi PA, Khodyuk IV. 2011. Optical and Luminescence Properties of Zinc Oxide (Review). 5, *Condensed matter*, Vol. 11, pp. 814-824.
3. Nagayasamy N, Gandhimathination S, Veerasamy V. 2013. The Effect of ZnO Thin Film and Its Structural and Optical Properties Prepared by Sol-Gel Spin Coating Method. *Open Journal of Metal*, Vol. 3, pp. 8-11.
4. Janardhan E, Reddy MM, Reddy PV, Reddy MJ. 2017. Synthesis of ZnO Nanoparticles - A Hydrothermal Protocol. 6, *European Journal of Applied Sciences*, Vol. 9, pp. 312-314.
5. Muhammad A, Ili RR, Faisal G, Shams U-R, Faheem BK, Rafaqat H. 2018. Continuous facile synthesis of nano-sized zinc oxide and its optical properties. 7, *Materials Research Express*, Vol. 5.
6. Huang J, Yin Z, Zheng Q. 2011. Applications of ZnO in organic and hybrid solar cells. *Applied Physics*, Vol. 4, pp. 3861-3877.
7. Soni BH, Deshpande MP, Bhatt SV, Garg N, Chaki SH. 2013. Studies on ZnO Nanorods Synthesized by Hydrothermal Method and their Characterization. 4, *Journal of nano- and electronic Physics*, Vol. 5, pp. 04077(1-6).
8. Chung FH. 1974. *Journal of Applied Crystallography*. Vol. 7, p. 519.
9. Cullity BD. 1978. *Elements of X-ray diffraction*. s.l. : Addison-Wesley Pub. Co, p. 555.
10. Mohan S, Vellakkat M, Aravind A, Reka U. 2020. Hydrothermal synthesis and characterization of Zinc Oxide nanoparticles of various shapes under different reaction conditions, *Nano Express*, Vol. 030028, pp. 1-15.
11. Suryanarayana C, Norton MG. 1998. *Determination of Crystallite Size and Lattice Strain. X-Ray Diffraction*. New York: Springer Science+Business Media, pp. 207-221.
12. Muhammad BL, Cummings F. 2019. Nitrogen plasma treatment of ZnO and TiO_2 nanowire arrays for polymer photovoltaic applications, *Surfaces, and Interfaces*, Vol. 17, p. 100382.
13. Alias SS, Ismail AB, and Mohamad AA. 2010. Effect of pH on ZnO nanoparticle properties synthesized by sol-gel centrifugation. 2, *Journal of Alloys and Compounds*, Vol. 499, pp. 231-237.
14. Noh Y-J, Na S-I, Kim S-S. 2013. Inverted polymer solar cells including ZnO electron transport layer fabricated by facile spray pyrolysis, *Solar energy materials, and solar cells*, Vol. 117, pp. 139-144.